Synchronization of strongly interacting alkali-metal spins

Or Katz[1,2,*] and Ofer Firstenberg[1]

[1]*Department of Physics of Complex Systems, Weizmann Institute of Science, Rehovot 76100, Israel*
[2]*Rafael, Ltd., IL-31021 Haifa, Israel*

The spins of gaseous alkali-metal atoms are commonly assumed to oscillate at a constant hyperfine frequency, which for many years has been used to define a standard unit of time, the second. Indeed, under standard experimental conditions, the spins oscillate independently, only weakly perturbed and slowly decaying due to random spin-spin collisions. Here we consider a different, unexplored regime of very dense gas, where collisions, more frequent than the hyperfine frequency, dominate the dynamics. We find that the hyperfine oscillations become significantly longer lived, and their frequency becomes dependent on the state of the ensemble, manifesting strong nonlinear dynamics. We reveal that the nonlinearity originates from a many-body interaction which synchronizes the electronic spins, driving them into a single collective mode. The conditions for experimental realizations of this regime are outlined.

I. INTRODUCTION

Binary collisions are a fundamental relaxation mechanism in atomic spin ensembles. During a collision, a pair of atoms within the ensemble briefly interacts, and its mutual electronic wave function is altered. Since the impact parameters are random, the quantum state of the ensemble relaxes at a rate R, proportional to the collisions rate Γ [1]. This prevailing relaxation mechanism limits the sensitivity of shot-noise-limited atomic sensors [2], such as magnetometers [3,4], gyroscopes [5], accelerometers [6], and clocks [7–11]. It is often desirable to increase the density of the ensemble in order to either increase the signal-to-noise ratio or allow for miniaturization of the device. However, with the increased density, the collisional relaxation rate $R \sim \Gamma$ increases, yielding no improvement in the sensor sensitivity [2].

Polarized alkali-metal ensembles were shown to overcome this limit at low magnetic fields [12–14]. When the Zeeman splitting ω_B satisfies $\omega_B \ll \Gamma$, the magnetic Zeeman coherences undergo a process akin to motional narrowing via frequent spin-exchange collisions. The relaxation rate is reduced to $R \sim \omega_B^2/\Gamma$ and so is the magnetic linewidth. This effect, denoted as spin-exchange relaxation free (SERF), stimulated the development of SERF magnetometers with unprecedented sensitivities [15].

While the SERF effect protects the Zeeman coherences at high atomic densities, the hyperfine coherences widely used for quantum information applications [16–18], radio astronomy [19], and atomic clocks [7–11] are subject to rapid relaxation rates $R \sim \Gamma$. Based on previous works which neglected the nonlinearity of the spin-exchange interaction [12], it is widely accepted that increased density yields faster hyperfine decoherence. In this paper, we prove the opposite. We derive the collisional dynamics of a dense ensemble and find that

the hyperfine coherence time increases significantly at high densities. We further show that rapid spin-exchange collisions synchronize the individual spins to a single frequency, which depends on the collective spin magnitude, leading to a unique nonlinear many-body dynamics.

II. MODEL

Consider first a toy model of N alkali-metal atoms, the ground level of which encompasses an electronic spin $S = 1/2$ and a nuclear spin $I = 1/2$. Most standard models describe the spin state and interactions with an effective ensemble-averaged set of equations [1,12,20,21]. Here we generalize these derivations and describe the many-body dynamics of the different atoms using a general master equation formalism of open quantum systems (see Appendix A for the full derivation). The atomic state of the nth atom is described by the observables of electronic spin $\mathbf{S}_n$, nuclear spin $\mathbf{I}_n$, and hyperfine coherence $\mathbf{A}_n \equiv \mathbf{S}_n \times \mathbf{I}_n$. The electrons are internally coupled to their nuclei by the hyperfine interaction $\omega_n \mathbf{S}_n \cdot \mathbf{I}_n$, while every pair of electrons $\mathbf{S}_n$, $\mathbf{S}_m$ experiences spin-exchange interaction at a time-averaged rate Γ_{mn}. At time scales longer than the time between collisions $\sim(\sum_m \Gamma_{mn})^{-1}$, the coherences between different atoms average to zero due to the randomness of collisions [1]. The many-body dynamics of the atoms can then be represented by a compact set of $9N$ nonlinear first-order Bloch equations:

$$\frac{d}{dt}\langle \mathbf{S}_n \rangle = \omega_n \langle \mathbf{A}_n \rangle + \sum_m \Gamma_{mn}(\langle \mathbf{S}_m \rangle - \langle \mathbf{S}_n \rangle), \quad (1)$$

$$\frac{d}{dt}\langle \mathbf{I}_n \rangle = -\omega_n \langle \mathbf{A}_n \rangle, \quad (2)$$

$$\frac{d}{dt}\langle \mathbf{A}_n \rangle = -\frac{\omega_n}{2}(\langle \mathbf{S}_n \rangle - \langle \mathbf{I}_n \rangle) - \sum_m \Gamma_{mn}\langle \mathbf{A}_n \rangle \quad (3)$$

$$+ \sum_m \Gamma_{mn}\langle \mathbf{S}_m \rangle \times \langle \mathbf{I}_n \rangle.$$

---

*Corresponding author: or.katz@weizmann.ac.il

The first term in Eqs. (1)–(3) describes the hyperfine precession of $\langle \mathbf{S}_n \rangle$ and $\langle \mathbf{I}_n \rangle$ through the coupling with the hyperfine-coherence vector $\langle \mathbf{A}_n \rangle$. The second term in Eq. (1) describes the collisional exchange between the nth electronic spin and all its neighbors. This term tends to synchronize all $\langle \mathbf{S}_n \rangle$ by equilibrating them with the other electronic spins $\langle \mathbf{S}_m \rangle$. In Eq. (3), the second term describes a decay of the hyperfine coherences at a rate $\sum_m \Gamma_{mn}$, and the last term describes the nonlinear coherence buildup, a result of the *spin-conservative* part of the collisional interaction.

Spin may be exchanged between atoms when they collide, but their total spin is conserved. Defining the atomic spin operators $\mathbf{F}_n = \mathbf{S}_n + \mathbf{I}_n$, we find from Eqs. (1)–(3) that the total spin of the ensemble $\langle \mathbf{F} \rangle \equiv \sum_n \langle \mathbf{F}_n \rangle$ is constant. In practice, this property holds for time scales shorter than the *spin destruction* rate of the ensemble (see Appendix B). As no external magnetic field is included, the model is isotropic, and the constant $\langle \mathbf{F} \rangle$ essentially sets a preferred direction.

III. MEAN-FIELD SOLUTION

We first consider the mean-field solution of Eqs. (1)–(3), assuming that $\omega_n \to \omega$, $\Gamma_{mn} \to \Gamma/N$, and $\langle \mathbf{F}_n \rangle \to \langle \mathbf{F} \rangle$. It follows that $\langle \mathbf{S}_n \rangle = \sum_n \langle \mathbf{S}_n \rangle / N \equiv \langle \mathbf{S} \rangle$, satisfying

$$\langle \ddot{\mathbf{S}} \rangle + \Gamma \langle \dot{\mathbf{S}} \rangle + \omega^2(\langle \mathbf{S} \rangle - 1/2\langle \mathbf{F} \rangle) - \omega \Gamma \langle \mathbf{F} \rangle \times \langle \mathbf{S} \rangle = 0. \quad (4)$$

Since $\langle \mathbf{F} \rangle$ is constant, Eq. (4) is a set of three linear nonhomogeneous equations, the general solution of which is

$$\langle S_q \rangle = \frac{1}{2} \langle F_q \rangle + \sum_{i=1}^{2} a_i^q e^{-\lambda_i^q t}.$$

Here, the subscript $q = 0, \pm$ denotes the three directions $\hat{z}, (\hat{x} \pm i\hat{y})/\sqrt{2}$, with the $\hat{z}$ axis defined as the direction of the vector $\langle \mathbf{F} \rangle$, and the six coefficients a_i^q determine the weights of the modes and depend on the initial condition of the spins. The time-dependent dynamics are described by six complex eigenvalues

$$\begin{pmatrix} \lambda_{1,2}^0 \\ \lambda_{1,2}^+ \\ \lambda_{1,2}^- \end{pmatrix} = \frac{1}{2} \begin{pmatrix} -\Gamma \pm \sqrt{\Gamma^2 - 4\omega^2} \\ -\Gamma \pm \sqrt{\Gamma^2 + 4i\Gamma\omega|\langle \mathbf{F} \rangle| - 4\omega^2} \\ -\Gamma \pm \sqrt{\Gamma^2 - 4i\Gamma\omega|\langle \mathbf{F} \rangle| - 4\omega^2} \end{pmatrix}, \quad (5)$$

where $\lambda_{1,2}^0$, $\lambda_{1,2}^+$, and $\lambda_{1,2}^-$ are the eigenvalues of $\langle S_0 \rangle$, $\langle S_+ \rangle$, and $\langle S_- \rangle$, respectively. The real part of these eigenvalues, associated with the relaxation rate R, is shown in Fig. 1(a) for a partially polarized ensemble $|\langle \mathbf{F} \rangle| = 1/2$.

In standard hot vapor experiments, the alkali-metal densities are kept low, such that $\Gamma \ll \omega$. In this regime, the eigenvalues in (5) are approximately given by

$$\begin{pmatrix} \lambda_{1,2}^0 \\ \lambda_1^{\pm} \\ \lambda_2^{\pm} \end{pmatrix} \approx \begin{pmatrix} \pm i\omega - \Gamma/2 \\ \pm i\omega - (1 - |\langle \mathbf{F} \rangle|)\Gamma/2 \\ \pm i\omega - (1 + |\langle \mathbf{F} \rangle|)\Gamma/2 \end{pmatrix}. \quad (6)$$

The oscillation frequency of the hyperfine coherences $|\mathrm{Im}(\lambda)| = \omega$ is constant. The relaxation rate of the $\lambda_{1,2}^0$ modes, associated with the so-called clock transition $(0 - 0)$ used by atomic frequency standards [7,9,10], is $R = \Gamma/2$. The end resonances relax at $R = (1 - |\langle \mathbf{F} \rangle|)\Gamma/2$, leading to the well-known line narrowing for $|\langle \mathbf{F} \rangle| \to 1$ [11].

In the strong-interaction regime $\Gamma \gg \omega$, the hyperfine oscillation is strongly perturbed by spin-exchange collisions, and the eigenvalues in (5) become

$$\begin{pmatrix} \lambda_2^0 \\ \lambda_1^0 \\ \lambda_2^{\pm} \\ \lambda_1^{\pm} \end{pmatrix} \approx \begin{pmatrix} -\Gamma \\ -\omega^2/\Gamma \\ \pm i\omega|\langle \mathbf{F} \rangle| - \Gamma \\ \pm i\omega|\langle \mathbf{F} \rangle| - (1 - |\langle \mathbf{F} \rangle|^2)\omega^2/\Gamma \end{pmatrix}. \quad (7)$$

We find that the relaxation of the $\lambda_1^{\pm,0}$ modes scales as ω^2/Γ, which we attribute to motional narrowing; increasing the collision rate Γ slows down the hyperfine decoherence. We denote this property as hyper-SERF, as the hyperfine coherences become free from spin-exchange relaxation. Furthermore and quite uniquely, the hyperfine frequency becomes dependent on the absolute magnitude of the spin $|\langle \mathbf{F} \rangle|$. The modified frequency of the $\lambda_{1,2}^{\pm}$ modes, shown in Fig. 1(b), is given by $\omega|\langle \mathbf{F} \rangle|$. On the other hand, the $\lambda_{1,2}^0$ modes have no oscillatory terms, indicating that the 0-0 clock-transition will "stop ticking."

IV. MANY-BODY SPIN DYNAMICS

To understand the nature of this mechanism, we generalize the mean-field result by numerically solving Eqs. (1)–(3) and obtaining the many-body dynamics of the spins. The initial values of $\langle \mathbf{S}_n \rangle$, $\langle \mathbf{I}_n \rangle$, $\langle \mathbf{A}_n \rangle$ are derived from the initial density matrices of the atoms ρ_n. We start with an optically pumped vapor in a spin-temperature distribution $\tilde{\rho}_n = \exp(-\beta F_n^z)/Z$, where $0 \leqslant \beta \leqslant 1$ determines the degree of polarization, and Z is a normalization factor [21]. To generate initial hyperfine coherences, we perturb $\tilde{\rho}_n$ by tilting the electronic spins by angles θ_n^y, θ_n^z and the nuclear spins by angles ϕ_n^y, ϕ_n^z, such that $\rho_n = U_n \tilde{\rho}_n U_n^\dagger$ with the rotation matrices

$$U_n = e^{i\theta_n^z S_z} e^{i\theta_n^y S_y} e^{i\phi_n^z I_z} e^{i\phi_n^y I_y}.$$

We first simulate the mean-field solution for $N = 100$, $\omega_n = \omega$, and $\Gamma_{mn} = \Gamma/N$, as shown in Fig. 2. The initial conditions are given by $\theta_n^z = \phi_n^y = \phi_n^z = 0$, $\theta_n^y = \pi/8$, and $\beta = 0.51$ ($|\langle \mathbf{F} \rangle| = 1/4$). We find indeed that the coherence time of the mean spin $\langle S_x \rangle$ is improved at high collision rate Γ. We further simulate
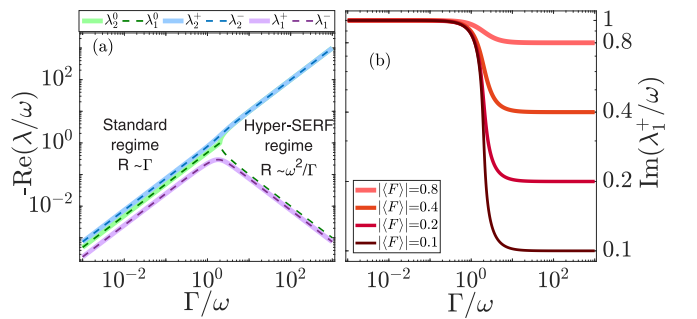

FIG. 1. (a) Relaxation rates of the hyperfine coherences for $I = 1/2$ and $|\langle \mathbf{F} \rangle| = 1/2$. At high collision rates $\Gamma \gg \omega$ (high densities), the relaxation of the $\lambda_1^{\pm,0}$ modes decreases. (b) Modified hyperfine frequencies. At high collision rates, the oscillation frequency of the hyperfine coherences becomes linearly dependent on the magnitude of the spin $|\langle \mathbf{F} \rangle|$.
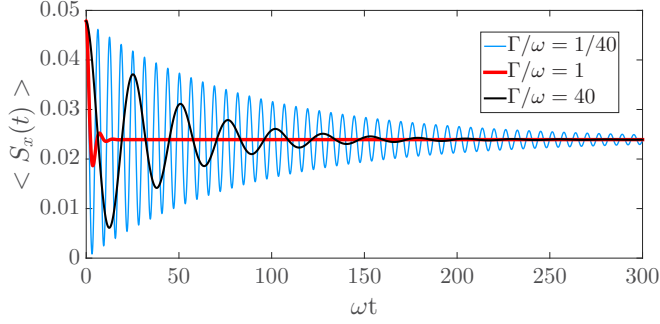
FIG. 2. Numerical simulation of the mean-field case. The coherence time revives at high densities $\Gamma \gg \omega$.

the many-body dynamics of the spins for unequal initial values and unequal interaction strengths ω_n and Γ_{mn}. We set $\beta = 0.73$ ($|\langle F \rangle| = 0.32$), $\theta_n^y, \theta_n^z \sim \mathcal{N}(\pi/3, \pi/15)$, $\phi_n^y, \phi_n^z \sim \mathcal{N}(\pi/6, \pi/30)$, randomly sampled from a normal distribution $\mathcal{N}(\mu, \sigma)$ with mean μ and standard deviation σ, resulting with unequal initial spin orientations. The collision rates $\Gamma_{mn} = \Gamma p_{mn}$ are set by generating a random double stochastic matrix p_{mn}. For the generality of the model, we also allow a spread for the atomic hyperfine frequencies $\omega_n \sim \mathcal{N}(\omega, \omega/50)$. In the standard, low-density, regime ($\Gamma \ll \omega_n$), the individual electronic spins precess independently at their inherent frequencies ω_n, forming spiral trajectories around their local spin vectors $\langle \mathbf{F}_n \rangle$, as shown in Fig. 3. The local spin vectors slowly relax to their equilibrium state $\langle \mathbf{F}_n \rangle \rightarrow \langle \mathbf{F} \rangle = \frac{1}{N} \sum_n \langle \mathbf{F}_n \rangle$ due to spin-exchange collisions, at a rate $R \sim \Gamma/2$. As a result, the spin coherences decay, and the center of each spiral adiabatically follows $\langle \mathbf{F}_n \rangle$. The mean electronic spin $\frac{1}{N} \sum_n \langle S_x^n \rangle$ (black line in Fig. 3) decays faster than the individual spins $\langle S_x^n \rangle$. This results from an additional (inhomogeneous) dephasing of
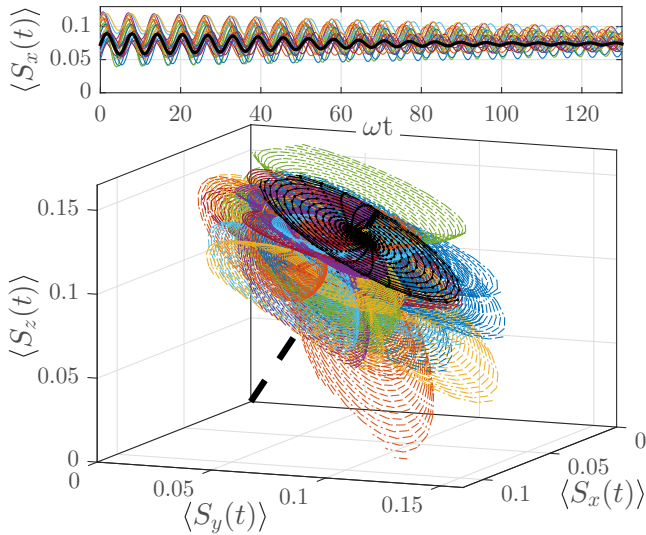

FIG. 3. Precession of the electronic spins in the standard, low-density regime with $\Gamma = \omega/100$ (25 out of $N = 100$ simulated spins are shown). Each electronic spin $\langle \mathbf{S}_n \rangle$ precesses independently around its local vector $\langle \mathbf{F}_n \rangle$, slowly decaying due to collisions. The mean electronic spin (black) precesses around the conserved spin $\langle \mathbf{F} \rangle$ (black dotted line), dephasing at an increased rate $R \sim \max(\Gamma, \Delta\omega)$.
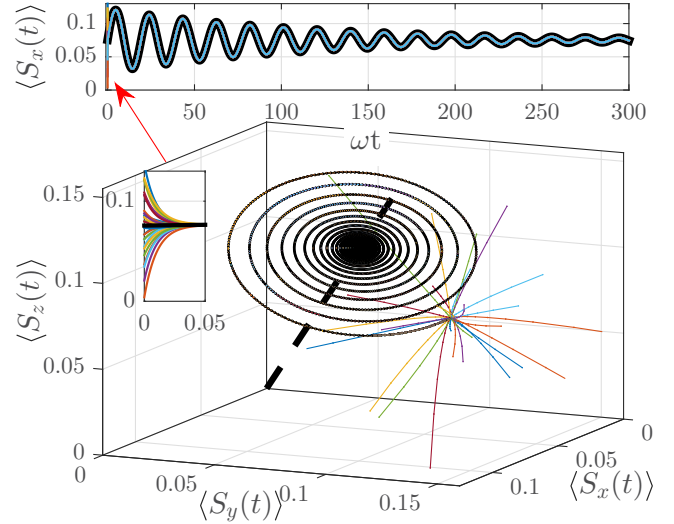

FIG. 4. Synchronization of the electronic spins in the strong-interaction regime with $\Gamma = 100\omega$ (25 out of $N = 100$ simulated spins are shown). The electronic spins synchronize rapidly after $t \sim \Gamma^{-1}$ to a common electronic mode (black). The electronic spins precess coherently at a modified, spin-dependent, frequency Ω and decay at a slow rate $R \sim \omega^2/\Gamma$.

the different hyperfine frequencies ω_n with a relaxation rate $R \sim [\sum_n (\omega_n - \omega)^2]^{1/2} \equiv \Delta\omega$.

In the strong-interaction regime ($\Gamma \gg \omega$), the electronic spins no longer precess individually, but rather synchronize to a single trajectory as shown in Fig. 4. All spins precesses around the mean spin $\langle \mathbf{F} \rangle$ with identical frequency of oscillation Ω. The synchronization time is rapid, scaling as Γ^{-1}.

V. SPIN SYNCHRONIZATION

To reveal the synchronization mechanism, we expand Eqs. (1)–(3) by the small parameter ω/Γ, keeping only second-order terms (see Appendix C):

$$\frac{d}{dt}\langle \mathbf{F}_n \rangle = \sum_m \Gamma_{mn}(\langle \mathbf{S}_m \rangle - \langle \mathbf{S}_n \rangle), \tag{8}$$

$$\frac{d}{dt}\langle \mathbf{S}_n \rangle \approx \sum_m \Gamma_{mn}(\langle \mathbf{S}_m \rangle - \langle \mathbf{S}_n \rangle) + \omega_n \langle \mathbf{F}_n \rangle \times \langle \mathbf{S}_n \rangle$$
$$- \frac{\omega_n^2}{\Gamma_n}(\langle \mathbf{S}_n \rangle - 1/2\langle \mathbf{F}_n \rangle). \tag{9}$$

This set of equations is known as the "tops model" [22], with $\omega_n \langle \mathbf{F}_n \rangle$ playing the role of a local external torque. The first term in Eq. (9) initially dominates and synchronizes the electronic spins over a transient time $\sim\Gamma^{-1}$, as shown in Fig. 4. Once the electronic spins are synchronized $\langle \mathbf{S}_m(t) \rangle \approx \langle \mathbf{S}_n(t) \rangle$, the spin vectors $\langle \mathbf{F}_n \rangle$ remain approximately constant [Eq. (8)]. The second term in Eq. (9) describes a local torque exerted on $\langle \mathbf{S}_n \rangle$ by the local field $\omega_n \langle \mathbf{F}_n \rangle$. We note that the directions and magnitudes of these local fields could be random. The third and least dominant term in Eq. (9) describes the slow relaxation of the electronic spin $\langle \mathbf{S}_n \rangle$ towards its steady value $\langle \mathbf{F}_n \rangle/2$ at the hyper-SERF rate ω_n^2/Γ_n. It is interesting to note that, although the electronic spins are frustrated by the different local fields

$\omega_n \langle \mathbf{F}_n \rangle$, the synchronization term overcomes this frustration in the strong-interaction regime. As a result, the synchronized electronic spins precess collectively around an effective mean field:

$$\mathbf{\Omega} \approx \frac{1}{N} \sum_n \omega_n \langle \mathbf{F}_n \rangle. \tag{10}$$

Hence electronic spins with random initial orientations are phase synchronized, and consequently precess coherently around the vector $\mathbf{\Omega}$, with a new collective modified hyperfine frequency Ω. Note that our result is valid also for the case of nonequal frequencies ω_n. This frequency depends on the polarization of the spin vectors $\langle \mathbf{F}_n \rangle$, recovering the mean-field results when $\omega_n = \omega$. Since the vectors $\langle \mathbf{F}_n \rangle$ do not synchronize, the directions of the nuclear spins $\langle \mathbf{I}_n \rangle$ remain unsynchronized as well. Nevertheless, the different nuclear spins process coherently, experiencing the slow electronic relaxation ω_n^2 / Γ_n.

It is also instructive to interpret our results from the viewpoint of collision-driven thermal equilibration, by extending the description of the SERF effect in Ref. [12] and considering the hyperfine interaction as an out-of-equilibrium term. At *low* atomic densities, spin-exchange collisions reduce the electron-nuclear coherence, as they redistribute the electronic spin between different atoms. At the same time, the hyperfine interaction strongly couples the nuclear spin to the electron spin within each atom. Consequently, the system is driven into a so-called spin-temperature distribution $\rho_n = \exp(-\vec{\beta}\mathbf{F}_n)/Z$ with no hyperfine coherence, thus maximizing the entropy of the spin degrees of freedom [23,24]. The mean thermalization rates of the different hyperfine coherences correspond to the decay rates of Eq. (6) (proportional to Γ). In contrast, at *high* atomic densities, the electron spins alone quickly thermalize (at a rate Γ) into a spin-temperature distribution $\rho_n^s = \exp(-\vec{\beta}_s \mathbf{S}_n)/Z_s$ through the spin-synchronizing term in Eq. (1). This thermalization leads to rapid loss of any initial correlations between the electronic and nuclear spins, making the electronic spins act as a single macroscopic magnetic moment on the nuclear spins $\langle \mathbf{A}_n \rangle \approx \langle \mathbf{S} \rangle \times \langle \mathbf{I}_n \rangle$. Application of this result to Eq. (1) shows that $|\vec{\beta}_s| = 2\mathrm{atanh}(2|\langle \mathbf{S} \rangle|)$ is constant in magnitude but processes according to $\partial_t \hat{\beta}_s = \hat{\beta}_s \times \mathbf{\Omega}$, i.e., the electronic spins oscillate around the modified hyperfine vector $\mathbf{\Omega}$. In turn, the nuclear spins precess around the electronic spin $\langle \mathbf{S} \rangle$ as suggested by Eq. (2), also with a precession frequency $\mathbf{\Omega}$. Full thermalization of the nuclear spins happens slowly, at an approximate rate $\sim\Gamma(\omega/\Gamma)^2$, where $(\omega/\Gamma)^2$ is the small angular loss during the synchronization time, similar to the loss in the standard SERF effect of the Zeeman coherences [12].

Our model predicts several new physical phenomena in the strong-interaction regime $\Gamma \gg \omega$. The first prediction is the motional narrowing of the hyperfine coherence, leading to its slow relaxation with a rate that scales as ω^2/Γ rather than Γ. The second prediction of the model is the nonlinear splitting of the hyperfine levels, "dressed" by the collisional interaction, such that both electronic and nuclear spins should process at a rate $\omega\langle|\mathbf{F}|\rangle$. The splitting depends linearly on the magnitude of the spin, and should therefore vary for different optical-pumping rates. This dependence can thus lead to intriguing nonlinear behavior when the probing scheme inherently involves optical pumping, such as in coherent
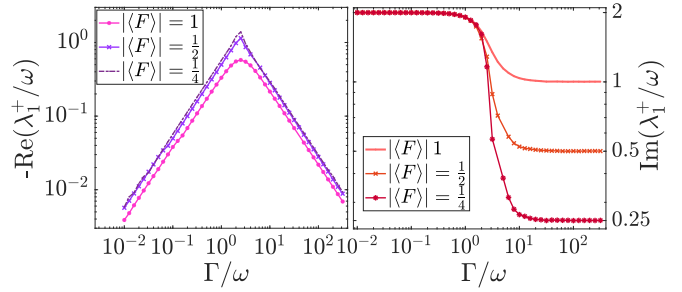

FIG. 5. Numerical calculation of the hyper-SERF effect for $I = 3/2$, for different initial polarizations $|\langle \mathbf{F} \rangle|$. Shown are the dominant relaxation rate of $\langle S_x \rangle$ (left) and its frequency (right). The results are qualitatively similar to the $I = 1/2$ case (note that here the maximal spin is $|\langle \mathbf{F} \rangle| = 2$).

population trapping [25]. A third prediction pertains to the case of nonzero bandwidth $\Delta\omega$. For alkali-metal ensembles, a mixture of different species with different hyperfine frequencies ω_n effectively features nonzero $\Delta\omega$. In these hybrid ensembles, the electronic spins of all species would synchronize and oscillate in a common mode. The synchronization mechanism can be optically probed by measuring the oscillation frequency of each species separately [26].

We analyzed above a toy model with $I = 1/2$ and no magnetic field ($\vec{B} = 0$). To verify that the hyper-SERF features persist for $I > 1/2$ we numerically solved the master equation [Eq. (A4)]. Figure 5 presents the dominant relaxation rate and frequency of $\langle S_x \rangle$ for atoms with $I = 3/2$, initialized with $\theta^z = \phi^y = \phi^z = 0$, $\theta^y = \pi/8$. These results show that the toy model results are qualitatively valid for $I > 1/2$ spins. If a magnetic field is applied, both the direction and magnitude of $\langle \mathbf{F} \rangle$ could vary in the presence of collisions. At magnetic fields $B \lesssim 10$ G, the Zeeman splitting is small ($g_s B \ll \omega$, where g_s is the gyromagnetic ratio), $\langle \mathbf{F} \rangle$ slowly precesses around $\vec{B}$, and our solution for the hyperfine coherences adiabatically follows the instantaneous $\langle \mathbf{F} \rangle$.

VI. EXPERIMENTAL ROADMAP

The hyper-SERF effect with $I = 3/2$ can be experimentally realized using ^{41}K, which has the lowest hyperfine frequency $2\omega_K \sim 254\,(2\pi)$ MHz (the factor of 2 enters since $I = 3/2$). The density required for entering the strong-interaction regime is $n_K > \omega_K/(\sigma_{SE}\bar{v}) \approx 5 \times 10^{17}$ cm^{-3}, where $\bar{v} \approx 10^5$ cm/s is the mean thermal velocity at $T \approx 600\,^{\circ}$C and $\sigma_{SE} = 1.5 \times 10^{-14}$ cm^2 is the spin-exchange cross section. High-temperature cells based on sapphire windows were demonstrated [27], as sapphire can withstand alkali metal at elevated temperatures for long time.

To observe hyper-SERF dynamics, relaxation mechanisms of the vapor should be kept low with respect to the hyperfine frequency. We propose to utilize a miniature cell of length $L = 100$ μm with 1 amagat of N_2 buffer gas at $T = 620\,^{\circ}$C (corresponding to $n_K = 2.1 \times 10^{18}$ cm^{-3} and $R_{SE} = 3.2 \times 10^9$ s^{-1}). Estimation of the main relaxation mechanisms of the vapor based on the theory in Refs. [28,29] yields $R_{SD} < 5 \times 10^6$ s^{-1} (see Appendix B), so that spin exchange dominates. The N_2 buffer gas can mitigate both the interaction with the walls

and other molecular relaxations. Choosing N_2 also enables efficient optical pumping at elevated densities, by quenching excited-state alkali-metal atoms and, consequently, avoiding spontaneous emission of stray photons [30]. An effective optical depth of ~ 700 is expected, with an optical linewidth of ~ 70 GHz dominated by alkali-metal self-broadening [31] and pressure broadening. At these conditions the probability to spontaneously radiate a photon is kept low ($\sim 0.2\%$), and the photon multiplicity is moderate (~ 30), mitigating radiation trapping [30]. Optical pumping at a rate of up to $R_P \approx 1$ GHz can be realized with a circularly polarized laser beam at the 1-W level, tuned near the D_1 resonance line and covering the entire miniature cell. High spin polarization $|\langle \mathbf{S} \rangle| = \frac{1}{2} R_P/(R_P + R_{SD})$ could be reached, even in the presence of a small molecular background that will be pumped through chemical-exchange collisions [32]. R_P can be experimentally varied (e.g., by detuning the pumping light from resonance) to verify the theoretical dependence on the spin polarization $|\langle \mathbf{F} \rangle|$. The magnetic field should be either zeroed or aligned with the optical-pumping axis for both efficient pumping and zeroing of the Zeeman coherences. Initial excitation of the hyperfine coherence, in low magnetic fields, can be realized by application of a magnetic field pulse which rotates the electron spin with little direct effect on the nuclear spin (see Appendix B). The spins can be monitored using standard schemes (e.g., absorption spectroscopy or off-resonant Faraday rotation) using fast photodiodes, as the susceptibility of the vapor strongly depends on the hyperfine coherence [33]. Fast optical modulators [34] can be used to switch off the optical pump beam, eliminating pump-induced relaxation during the measurement.

VII. CONCLUSION

In conclusion, we have shown that at high spin-exchange rates the oscillation frequency of the hyperfine coherence is no longer constant. Instead, many-body interactions govern the dynamics of the spins, resulting in a collectively synchronized and surprisingly coherent spin state. Operation at high alkali-metal densities along with maturity of miniaturized high-temperature cells could lead to the emergence of highly sensitive or highly nonlinear applications in small-scale devices. These include, for example, miniature SERF magnetometers for geomagnetic fields and potentially new applications of multiphoton processes such as coherent population trapping.

APPENDIX A: DERIVATION OF THE MANY-BODY MASTER EQUATIONS

The dynamics of dense thermal alkali-metal spins is usually described by a *mean* density matrix $\bar{\rho}$ satisfying the Liouville

equation [1,20]. This evolution yields the average spin properties of the gas. Including the spin-exchange interaction, this equation is given by [see Eq. (10.20) in [1]]

$$\partial_t \bar{\rho} = -\frac{i}{\hbar}[H_0, \bar{\rho}] + \Gamma \langle \mathcal{S}_c \bar{\rho} \mathcal{S}_c^\dagger - \bar{\rho} \rangle_c, \qquad (A1)$$

where H_0 is the single-atom hyperfine interaction Hamiltonian, and $\mathcal{S}_c$ is the alkali-metal–alkali-metal scattering matrix for a specific collision event, characterized with a particular set of collisional parameters (including the impact parameter, the orbital plane, and the instantaneous velocity) which are labeled with a subscript "c". Γ is the mean collision rate and $\langle \cdots \rangle_c$ denotes an ensemble average over the possible collisional realizations.

Here we generalize this equation to describe the many-body dynamics of $N \ggg 1$ different spins, which would finally yield Eqs. (1)–(3). We define ρ as the global density matrix of the vapor, describing the state of the N electronic and N nuclear spins in the electronic ground state. Spin-exchange collisions of alkali-metal atoms are binary and sudden [1], such that after a collisional event c between the mth and nth atoms the density matrix evolves as $\rho \rightarrow \mathcal{S}_c^{(mn)} \rho \mathcal{S}_c^{(mn)\dagger}$ where $\mathcal{S}_c^{(mn)}$ is the scattering matrix of the c collisional event, operating on the bipartite state of the density matrix within the mth and nth atomic subspace. On average, the many-body density matrix of the spins ρ would evolve as

$$\rho(t + dt) = -\frac{i}{\hbar}[\mathcal{H}_0, \rho]dt + \sum_{m,n} \sum_c p_c^{mn}(dt) \mathcal{S}_c^{(mn)} \rho \mathcal{S}_c^{(mn)\dagger}$$
$$+ \left[1 - p_c^{mn}(dt)\right]\rho(t).$$

Here the first term describes the unitary evolution of the spins with $\mathcal{H}_0 = \hbar \sum_n \omega_n \mathbf{I}_n \cdot \mathbf{S}_n$ being the hyperfine Hamiltonian of all particles. The second term describes the collisional interaction between the particles: $p_c^{mn}(dt)$ is the probability that a specific pair of atoms m and n had collided during a time interval dt where c labels a set of specific collision parameters. $p_c^{mn}(dt)$ is determined by the kinetic theory of thermal atoms, and on average has a memoryless time dependence (see Chap. 12 in [35]) such that $p_c^{mn}(dt) = [1 - \exp(-\Gamma dt)]\tilde{p}_c^{mn} \approx \tilde{p}_c^{mn} \Gamma dt$, where Γ is the hard-sphere collision rate and $\tilde{p}_c^{mn}$ depends on the relative distance and velocity of the two atoms and is nonzero when the atoms are close to each other (on the order of the mean free path). We then find the Liouville equation

$$\partial_t \rho = -\frac{i}{\hbar}[\mathcal{H}_0, \rho] + \Gamma \sum_{m,n} \sum_c \tilde{p}_c^{mn}(\mathcal{S}_c^{(mn)} \rho \mathcal{S}_c^{(mn)\dagger} - \rho),$$

$$(A2)$$

describing the state of the vapor for times shorter than other relaxation rates and spatial diffusion (see Appendix B). The collisional scattering matrix associated with strong spin-exchange collisions is manifested as a correlated two-spin rotation $\mathcal{S}_c^{(mn)} = \exp(i\delta_c \Pi_{mn}^e) = \cos(\delta_c) + i \sin(\delta_c)\Pi_{mn}^e$, where $\Pi_{mn}^e = \frac{1}{2} + 2\mathbf{S}_n \cdot \mathbf{S}_m$ is the exchange operator of the m-n spin pair, and δ_c is the phase accumulated during the specific collisional event [see Eq. (10.252) in [1]]. Substitution of this

scattering matrix in Eq. (A2) gives

$$\partial_t \rho = -\frac{i}{\hbar}[\mathcal{H}_0, \rho] + \Gamma \sum_{m,n} \sum_c \tilde{p}_c^{mn} \left(\frac{i}{2} \sin(2\delta_c)[\Pi_{mn}^e, \rho] \right.$$
$$\left. + \sin^2(\delta_c)(\Pi_{mn}^e \rho \Pi_{mn}^e - \rho) \right),$$

where the first term describes collision-induced frequency shifts and the second term describes real collisional exchange of the two spins. The phases δ_c can be estimated either with a partial-wave analysis or using a classical path analysis [12]. Upon ensemble averaging, we obtain the simpler equation

$$\partial_t \rho = -\frac{i}{\hbar}[\mathcal{H}_0, \rho] + \sum_{m,n} \Gamma_{mn}(\Pi_{mn}^e \rho \Pi_{mn}^e - \rho) \quad \text{(A3)}$$

where $\Gamma_{mn} \equiv \langle \Gamma \sum_c \tilde{p}_c^{mn} \sin^2(\delta_c) \rangle_c$ is the average spin-exchange rate of the atomic pair m-n. The frequency-shift term is omitted, since $\delta_c \gtrsim \pi$ such that, upon ensemble averaging, $\langle \sum_c \tilde{p}_c^{mn} \sin(2\delta_c) \rangle_c$ is negligible (see Fig. 10.8 in [1]). Direct substitution of the exchange operator $\Pi_{mn}^e = \frac{1}{2} + 2\mathbf{S}_n \cdot \mathbf{S}_m$ results in the generalized evolution equation

$$\partial_t \rho = -i \sum_n \omega_n[\mathbf{I}_n \mathbf{S}_n, \rho] + \sum_{m,n} \Gamma_{mn} \left(-\frac{3}{4} \rho \right.$$
$$\left. + \mathbf{S}_n \mathbf{S}_m \rho + \rho \mathbf{S}_n \mathbf{S}_m + 4 \mathbf{S}_n \mathbf{S}_m \rho \mathbf{S}_n \mathbf{S}_m \right).$$

We now assume that the quantum correlations developed between different colliding atoms during the interactions are rapidly lost. These coherences are assumed to be lost for time scales longer than the short collision duration (a few picoseconds) due to the randomness of the collision parameters and the random choice of colliding pairs [see both Eq. (10.105) in [1] and the discussion in Sec. IV.D.4 in [36]]. We therefore consider the case that the density matrix is interatomic separable and assume the simple form

$$\rho = \rho_1 \otimes \ldots \rho_n \ldots \otimes \rho_N,$$

where ρ_n is the reduced density matrix of the nth atom. Using this form, we derive the equation of motion for $\rho_n = \text{Tr}_{\neq n}(\rho)$ by partial tracing the state of all spins but n, yielding

$$\partial_t \rho_n = -i \omega_n[\mathbf{I}_n \cdot \mathbf{S}_n, \rho_n] + \sum_m \Gamma_{mn} \left(-\frac{3}{4} \rho_n \right.$$
$$\left. + \mathbf{S}_n \rho_n \mathbf{S}_n + \langle \mathbf{S}_m \rangle (\rho_n \mathbf{S}_n + \mathbf{S}_n \rho_n - 2i \mathbf{S}_n \times \rho_n \mathbf{S}_n) \right)$$
$$\text{(A4)}$$

where $\langle \mathbf{S}_m \rangle \equiv \text{Tr}(\rho_m \mathbf{S}_m)$ is the mean electronic spin of the mth atom, and ϵ_{ijk} is Levi-Civita symbol. Equation (A4) is the many-body generalization for the mean-field evolution of the spin-exchange interaction [see [37], in particular Eqs. (VI.8) and (VI.15)].

The evolution of the different moments $\langle S_n^i \rangle$, $\langle I_n^i \rangle$, and $\langle A_n^i \rangle$ in Eqs. (1)–(3) is then derived by calculating the expectation values using the density matrix formalism $\langle X_n \rangle = \text{Tr}(\rho_n X_n)$ and the commutation relations of the electronic spins $\{S_m^i, S_m^j\} = \frac{1}{2}\delta_{ij}$ and $[S_m^i, S_n^j] = i\delta_{mn}\epsilon_{ijk}S_k$ and the nuclear spins $\{I_m^i, I_m^j\} = \frac{1}{2}\delta_{ij}$ and $[I_m^i, I_n^j] = i\delta_{mn}\epsilon_{ijk}I_k$.

APPENDIX B: SPIN-RELAXATION MECHANISMS AND INITIALIZATION OF HYPERFINE COHERENCE

The dominant spin-relaxation mechanisms in the high-temperature atomic vapor we consider are [28] (a) interaction with the walls at a rate R_{wall}, (b) K-K destructive collisions at a rate R_{KK}, (c) molecular relaxation by singlet dimers $^1\Sigma_g^+$ at a rate R_S, and (d) spin rotation through collisions with N_2 at a rate R_{buff}. Other relaxation mechanisms, such as magnetic field gradients [21], can be made small. The total electronic relaxation rate is then given by

$$R_{\text{SD}} = R_{\text{wall}} + R_{\text{KK}} + R_S + R_{\text{buff}}.$$

We estimate the electronic relaxation R_{wall} by assuming that the walls are completely depolarizing and consider the least decaying diffusion mode [see Eq. (10.286) in [1]]

$$R_{\text{wall}} \approx 4\pi^2 Q D / L^2 \approx 10^6 \text{ s}^{-1},$$

where $D \approx 0.4 \text{ cm}^2/\text{s}$ is the diffusion coefficient for 1 amagat of N_2 and $Q = 6$ is the slowing down factor (for $I = 3/2$) accounting for the loss of nuclear spin during the interaction with the wall [see Eq. (10.271) in Ref. [1]]. Spin destruction of alkali-metal–alkali-metal collisions consists of two main mechanisms: spin rotation in binary collisions and spin-axis relaxation in molecular triplet dimers [29,38]. These two interactions were found to have equal magnitudes and together destruct the spin at a rate

$$R_{\text{KK}} = n_\kappa \sigma_{\text{KK}} \bar{v} \approx 2 \times 10^5 \text{ s}^{-1}$$

where we used $n_\kappa = 1.7 \times 10^{18} \text{ cm}^{-3}$, $\bar{v} \approx 10^5 \text{ cm/s}$ and we assumed the cross section $\sigma_{\text{KK}} = 10^{-18} \text{ cm}^{-2}$, which was measured at low temperatures [39], with no known dependence on temperature variation. The current theoretical models predict an order-of-magnitude smaller value for the σ_{KK} we use [29,38], and this cross section should be considered only as an order-of-magnitude estimate. To validate the molecular estimation at higher temperatures, we also compute the chemical potential for triplet dimers at $T = 620°$ C by following a procedure similar to Ref. [28] and using the molecular potential in [40]. We then estimate that the chemical equilibrium coefficient of the triplet dimers is $\mathcal{K}_T = 3 \times 10^{-23} \text{ cm}^3$, using a triplet binding energy of $D_e^{(T)} = 0.032 \text{ eV} < k_B T$ and assuming that during a molecular lifetime the spin loses a fraction $\alpha_T \leqslant 1$ of its coherence. The estimated triplet destruction at $T = 620°\text{C}$ is then bounded by $R_{\text{KK}} \approx \alpha_T \tau_c^{-1} \mathcal{K}_T n_\kappa < 3 \times 10^6 \text{ s}^{-1}$, where $\tau_c^{-1} = n_{N2}(\sigma \bar{v})_{\text{K2-N2}} \approx 6 \times 10^{10} \text{ s}^{-1}$ is the hard-sphere collision rate with N_2 molecules (which serve as third bodies).

Singlet dimers are the most populated molecular state, with estimated dimer to monomer ratio limited to a few percent at $T = 620°\text{C}$. (Using measured data of the molecular partial pressure of K_2 by Ref. [41] we estimate a molecular fraction of 3.5%, and using the potentials of Ref. [40] we numerically calculate the chemical potential following a similar procedure to Ref. [28] and estimate a fraction of 5%. We verify that our chemical potential fits the results of Ref. [28] at low temperatures.) We note, however, that the molecular fraction calculated here could be larger for alkali-metal halides, and therefore pure alkali metal should be used instead [41]. The atomic decoherence due to singlet dimers results mainly

from molecular dissociation, where relaxation of the nuclear spins during a molecular lifetime is found negligible. Upon dissociation of the dimer, the total spins of the atomic pair are conserved but the atoms could possibly result in hyperfine coherence being unsynchronized with the rest of the atomic ensemble. Such atoms would spin thermalize with the rest of the ensemble and contribute to the total decoherence rate. We approximate this rate by

$$R_S = \alpha_S \left(\frac{n_{K2}}{n_K} \right) \tau_c^{-1} \exp\left(-\frac{D_e^{(S)}}{k_B T} \right) < 1.5 \times 10^6 \text{ s}^{-1}$$

where $D_e^{(S)} \approx 0.55$ eV is the molecular binding energy, n_{K2} is the density of singlet dimers, and $\alpha_S \leqslant 1$ is the amount of coherence lost at a single dissociation of a singlet dimer. The singlet dimers have no electronic spin and during their lifetime only the nuclear spin is subject to relaxation. The nuclear spin is subject to both electric-quadruple and nuclear spin interactions [28]. As a singlet molecule experiences multiple collisions before dissociation, the nuclear spin relaxation is given by $R_s^{(1)} \approx (\frac{2}{3}\Omega_q^2 + c^2\langle J^2 \rangle)\tau_R < 10 \text{ s}^{-1}$ where $\Omega_q \approx 1.9 \times 10^5 \text{ s}^{-1}$ is the quadruple interaction strength, $c\sqrt{\langle J^2 \rangle} \approx 3.5 \times 10^4 \text{ s}^{-1}$ is the spin rotation interaction strength, and τ_R is the typical reorienting collision time. In our setup τ_R is equally split between collisions with buffer gas atoms, which reorient the molecular rotation (J), and chemical-exchange collisions with other alkali-metal atoms, which swap the nuclear spin of one of the nuclei (which is equivalent to reorientation of the nuclear spin) such that overall $\tau_R^{-1} \approx [n_{N2}(\sigma_J \bar{v})]^{-1} + [n_K(\sigma \bar{v})_{K\text{-}K}]^{-1} \approx 6 \times 10^9 \text{ s}^{-1}$, where we used the chemical-exchange rate $(\sigma \bar{v})_{K\text{-}K2} \approx 1.5 \times 10^{-9} \text{ cm}^3/\text{s}$ and the reorientation rate $\sigma_J \bar{v}_{K2\text{-}N2} \approx 1.5 \times 10^{-10} \text{ cm}^3/\text{s}$ based on measurements with Rb_2 dimers [28]. We note that atomic potassium encounters also frequent chemical-exchange collisions with singlet dimers, at a rate $R_{CE} = n_{K2}(\sigma \bar{v})_{K\text{-}K2} \approx 7.5 \times 10^7 \text{ s}^{-1}$, which, in contrast to R_S, is not suppressed with the Boltzmann factor $\exp(-D_e^{(S)}/k_B T)$ [42]. These collisions conserve the electronic spin and can be thought of as an exchange operation of one atomic nucleus with one of the nuclei in a molecule. The molecular nuclei, previously formed from a pair of atomic alkali metals, are oriented with almost the same direction as the alkali-metal one. Therefore, the chemical-exchange collisions play a similar role to atomic spin-exchange collisions, and its effect on the atomic vapor is to increase R_{SE} but not R_{SD}. Therefore in the strong-interaction regime it should not impose any additional relaxation. We note that application of high magnetic fields can significantly suppress the dimer part of the relaxation, for both the singlet and triplet states [29]. Relaxation due to collisions with buffer gas is estimated as

$$R_{buff} = n_{N2}\sigma' \bar{v}' < 10^4 \text{ s}^{-1}$$

where $n_{N2} = 2.5 \times 10^{19} \text{ cm}^{-3}$ is the nitrogen density, $\sigma' \approx 10^{-21} \text{ cm}^2$ is the spin-rotation cross section of K-N_2 estimated at $T = 620\,^\circ$C (with the $T^{3.7}$ dependence taken into account),

and $\bar{v}' \approx 1.3 \times 10^5$ cm/s is the mean thermal velocity of the K-N_2 pair [1]. In conclusion, for the experimental conditions considered here we predict $R_{SD} < 5 \times 10^6 \text{ s}^{-1}$, such that spin exchange is expected to be the dominant relaxation mechanism even for very dense vapor at high temperatures.

Initial excitation of the hyperfine coherence, in low magnetic fields, can be realized by application of a magnetic-field pulse which rotates the electron spin (which has a gyromagnetic ratio $g_s = 2.8$ MHz/G) with little direct effect on the nuclear spin (which has a gyromagnetic ratio of $g_I = 78$ Hz/G for ^{41}K [43]). A general pulse would excite simultaneously both Zeeman and hyperfine coherences. It is possible, however, to excite a specific hyperfine coherence magnetically while leaving the Zeeman coherence unexcited by shaping the applied magnetic pulse. For example, if the pulsed magnetic field is oriented perpendicular to the optical-pumping axis, and consists of a single sine burst [$B_\perp \sin(\omega_B t)$ for $0 \leqslant t \leqslant 2\pi/\omega_B$], then it would rotate the electronic spin back and forth. For $\omega_B < \omega_K$ the nuclear spin is strongly coupled to the electronic spin and follows its track such that at the end of the pulse the spins return to their starting point, and no coherence is introduced. If $\omega_B > \omega_K$ only the electronic spin precesses by the pulse and the hyperfine interaction with I accumulates an additional phase (azimuth $\sim \omega_K/\omega_B$, and elevation $\sim \frac{1}{4}g_s B_\perp/\omega_B$) and the spins would not return to their initial point, exciting mainly the λ_1^+ hyperfine coherence, while the Zeeman coherences are zeroed at the end of the pulse. Low inductance short wires can support gigahertz-bandwidth pulses and can be positioned in the proximity of the cell [44].

APPENDIX C: APPROXIMATIONS IN THE STRONG-INTERACTION REGIME

In this appendix, we derive Eqs. (8) and (9), which approximate the dynamics of the vapor in the strong-interaction regime $\sum_m \Gamma_{mn} \gg \omega_n$. We first transform the first-order differential equations (1)–(3) into second-order differential equations by eliminating the torque observable $\langle \mathbf{A}_n \rangle$:

$$\frac{d}{dt}\langle \mathbf{S}_n \rangle = -\frac{d}{dt}\langle \mathbf{I}_n \rangle + \sum_m \Gamma_{mn}(\langle \mathbf{S}_m \rangle - \langle \mathbf{S}_n \rangle), \quad \text{(C1)}$$

$$\frac{d^2}{dt^2}\langle \mathbf{I}_n \rangle + \sum_m \Gamma_{mn}\frac{d}{dt}\langle \mathbf{I}_n \rangle + \frac{\omega_n^2}{2}(\langle \mathbf{I}_n \rangle - \langle \mathbf{S}_n \rangle) \quad \text{(C2)}$$

$$+ \omega_n \sum_m \Gamma_{mn}\langle \mathbf{S}_m \rangle \times \langle \mathbf{I}_n \rangle = 0.$$

Equation (C1) can be used to derive Eq. (8), which describes the dynamics of the total spins $\langle \mathbf{F}_n \rangle = \langle \mathbf{S}_n \rangle + \langle \mathbf{I}_n \rangle$. In the strong-interaction regime, the oscillations slow down due to motional narrowing, rendering the second-order derivatives $\frac{d^2}{dt^2}\langle \mathbf{I}_n \rangle$ negligible. We furthermore assume that $\langle \mathbf{S}_m \rangle \approx \langle \mathbf{S}_n \rangle$ due to the synchronization of the spins. Defining the mean relaxation of the nth atom as $\Gamma_n \equiv \sum_m \Gamma_{mn}$ and substituting Eq. (8) into Eq. (C2) thus simplifies to Eq. (9).

[1] W. Happer, Y.-Y. Jau, and T. Walker, *Optically Pumped Atoms* (Wiley-VCH, Weinheim, 2010).

[2] J. Kitching, S. Knappe, and E. A. Donley, IEEE Sens. J. **11**, 1749 (2011).

[3] D. Sheng, S. Li, N. Dural, and M. V. Romalis, Phys. Rev. Lett. **110**, 160802 (2013).

[4] W. Wasilewski, K. Jensen, H. Krauter, J. J. Renema, M. V. Balabas, and E. S. Polzik, Phys. Rev. Lett. **104**, 133601 (2010).

[5] T. W. Kornack, R. K. Ghosh, and M. V. Romalis, Phys. Rev. Lett. **95**, 230801 (2005).

[6] G. W. Biedermann, H. J. McGuinness, A. V. Rakholia, Y.-Y. Jau, D. R. Wheeler, J. D. Sterk, and G. R. Burns, Phys. Rev. Lett. **118**, 163601 (2017).

[7] J. Vanier, Appl. Phys. B **81**, 421 (2005).

[8] J. Camparo, Phys. Today **60**(11), 33 (2007).

[9] S. Knappe, V. Shah, P. Schwindt, L. Hollberg, J. Kitching, L. Liew, and J. Moreland, Appl. Phys. Lett. **85**, 1460 (2004).

[10] S. A. Zibrov, I. Novikova, D. F. Phillips, R. L. Walsworth, A. S. Zibrov, V. L. Velichansky, A. V. Taichenachev, and V. I. Yudin, Phys. Rev. A **81**, 013833 (2010).

[11] Y.-Y. Jau, A. B. Post, N. N. Kuzma, A. M. Braun, M. V. Romalis, and W. Happer, Phys. Rev. Lett. **92**, 110801 (2004).

[12] W. Happer and A. C. Tam, Phys. Rev. A **16**, 1877 (1977).

[13] O. Katz, M. Dikopoltsev, O. Peleg, M. Shuker, J. Steinhauer, and N. Katz, Phys. Rev. Lett. **110**, 263004 (2013).

[14] O. Katz and O. Firstenberg, Nat. Commun. **9**, 2074 (2018).

[15] D. Budker and M. Romalis, Nat. Phys. **3**, 227 (2007).

[16] C. Shu, P. Chen, TKA. Chow, L. Zhu, Y. Xiao, M. M. T. Loy, and S. Du, Nat. Commun. **7**, 12783 (2016).

[17] D. J. Saunders, J. H. D. Munns, T. F. M. Champion, C. Qiu, K. T. Kaczmarek, E. Poem, P. M. Ledingham, I. A. Walmsley, and J. Nunn, Phys. Rev. Lett. **116**, 090501 (2016).

[18] K. Hammerer, A. S. Sørensen, and E. S. Polzik, Rev. Mod. Phys. **82**, 1041 (2010).

[19] H. I. Ewen and E. M. Purcell, Nature (London) **168**, 356 (1951).

[20] R. Karplus and J. Schwinger, Phys. Rev. **73**, 1020 (1948).

[21] S. Appelt, A. B.-A. Baranga, C. J. Erickson, M. V. Romalis, A. R. Young, and W. Happer, Phys. Rev. A **58**, 1412 (1998).

[22] F. Ritort, Phys. Rev. Lett. **80**, 6 (1998).

[23] L. W. Anderson, F. M. Pipkin, and J. C. Baird, Jr., Phys. Rev. **116**, 87 (1959).

[24] L. W. Anderson and A. T. Ramsey, Phys. Rev. **132**, 712 (1963).

[25] E. Arimondo, Prog. Opt. **35**, 257 (1996).

[26] O. Katz, O. Peleg, and O. Firstenberg, Phys. Rev. Lett. **115**, 113003 (2015).

[27] V. O. Lorenz, X. Dai, H. Green, T. R. Asnicar, and S. T. Cundiff, Rev. Sci. Instrum. **79**, 123104 (2008).

[28] S. Kadlecek, L. W. Anderson, C. J. Erickson, and T. G. Walker, Phys. Rev. A **64**, 052717 (2001).

[29] C. J. Erickson, D. Levron, W. Happer, S. Kadlecek, B. Chann, L. W. Anderson, and T. G. Walker, Phys. Rev. Lett. **85**, 4237 (2000).

[30] M. A. Rosenberry, J. P. Reyes, D. Tupa, and T. J. Gay, Phys. Rev. A **75**, 023401 (2007).

[31] J. J. Maki, M. S. Malcuit, J. E. Sipe, and R. W. Boyd, Phys. Rev. Lett. **67**, 972 (1991).

[32] M. P. Sinha, C. D. Caldwell, and R. N. Zare, J. Chem. Phys. **61**, 491 (1974).

[33] B. S. Mathur, H. Y. Tang, and W. Happer, Phys. Rev. A **2**, 648 (1970).

[34] JENOPTIK, Optik, Systeme GmbH, Jena, Germany, https://www.jenoptik.com/products/optoelectronic-systems/light-modulation/integrated-optical-modulators-fiber-coupled.

[35] F. Reif, *Fundamentals of Statistical and Thermal Physics* (McGraw-Hill, New York, 1965).

[36] C. Cohen-Tannoudji, J. Dupont-Roc, and G. Grynberg, *Atom-Photon Interactions* (Wiley, New York, 1992).

[37] W. Happer, Rev. Mod. Phys. **44**, 169 (1972).

[38] S. Kadlecek, T. Walker, D. K. Walter, C. Erickson, and W. Happer, Phys. Rev. A **63**, 052717 (2001).

[39] S. Kadlecek, L. Anderson, and T. Walker, Nucl. Instrum. Methods A **402**, 208 (1998).

[40] M. Krauss and W. Stevens, J. Chem. Phys. **93**, 4236 (1990).

[41] A. N. Nesmeyanov, *Vapor Pressure of the Chemical Elements*, translated by J. S. Carasso (Academic, New York, 1963).

[42] R. Gupta, W. Happer, G. Moe, and W. Park, Phys. Rev. Lett. **32**, 574 (1974).

[43] T. G. Tiecke, available online at http://www.tobiastiecke.nl/archive/PotassiumProperties.pdf (v1.02, May 2011).

[44] J. M. Nichol, T. R. Naibert, E. R. Hemesath, L. J. Lauhon, and R. Budakian, Phys. Rev. X **3**, 031016 (2013).